ISSN 0036-0236, Russian Journal of Inorganic Chemistry, 2022, Vol. 67, No. 5, pp. 670–682. © Pleiades Publishing, Ltd., 2022.
Russian Text © The Author(s), 2022, published in Zhurnal Neorganicheskoi Khimii, 2022, Vol. 67, No. 5, pp. 606–619.

PHYSICOCHEMICAL ANALYSIS OF INORGANIC SYSTEMS

Phase Equilibria in the $Cu_2Se–GeSe_2–SnSe_2$ System

L. F. Mashadieva[a, *], Z. M. Alieva[b], R. Dzh. Mirzoeva[c], Yu. A. Yusibov[b], A. V. Shevel'kov[d], and M. B. Babanly[a]

[a] *Institute of Catalysis and Inorganic Chemistry, National Academy of Sciences of Azerbaijan, Baku, Az-1143 Azerbaijan*
[b] *Ganja State University, Ganja, AZ-2000 Azerbaijan*
[c] *Baku State University, Baku, Az-1143 Azerbaijan*
[d] *Moscow State University, Moscow, 119991 Russia*
**e-mail: leylafm76@gmail.com*

Received July 16, 2021; revised December 25, 2021; accepted December 27, 2021

Abstract—Phase equilibria in the $Cu_2Se–GeSe_2–SnSe_2$ quasi-ternary system were studied by differential thermal analysis (DTA) and X-ray powder diffraction analysis. A series of polythermal sections, the 750-K isothermal section of the phase diagram, and the liquid surface projection were plotted. Primary crystallization and homogeneity areas of phases were determined, as well as the characters and types of invariant and monovariant equilibria. Extensive Cu_2GeSe_3-base and Cu_2SnSe_3-base solid solutions were found to exist in the system along the $Cu_2GeSe_3–Cu_2SnSe_3$ section.

Keywords: copper germanium tin selenides, phase diagram, liquidus surface, quasi-ternary system, solid solutions

DOI: 10.1134/S0036023622050126

INTRODUCTION

Copper chalcogenides and their based phases are among the most popular subject matters of research in semiconductor materials science; they have many functional properties showing a potential for use in several fields, such as photoelectrochemical, photocatalytic, and solar cells [1–5]. These phases attract increasing attention as promising thermoelectric materials due to their high efficiency, tunable transport properties, as well as the low toxicity and availability of their constituents [6–11]. In addition, copper chalcogenides are mixed electron–ionic conductors and, due to the high mobility of "liquid-like" copper ions, they exhibit record-breaking values of cationic conductivity (up to $\sim 3\ \Omega^{-1}\ cm^{-1}$) and ion diffusion ($\sim 10^{-5}\ cm^2/s$) [12–14]. This makes them promising materials for ion-selective electrodes or solid electrolytes in the development of various types of electric batteries, sensors, etc. [12–19].

It is well known that an efficient strategy for optimizing functional properties of the material is to modify its composition and structure. In order to search for and design new materials and for a better understanding of the relationships among the composition, structure, and properties, one needs to have reliable data on the phase equilibria and thermodynamic properties of the relevant multicomponent systems [19–22].

In our prior works [23–27], we carried out similar diligent studies of complex systems involving copper chalcogenides; we found new phases and determined their primary crystallization and homogeneity areas.

Here, we will present new experimental data on phase equilibria in the $Cu_2Se–GeSe_2–SnSe_2$ quasi-ternary system (system A). The ternary phases formed in this system (Cu_8GeSe_6, Cu_2SnSe_3, and Cu_2GeSe_3) have extensively been studied as thermoelectric materials [11–13].

The terminal compounds (Cu_2Se, $GeSe_2$, and SnSe) and boundary quasi-binary constituents ($Cu_2Se–GeSe_2$, $GeSe_2–SnSe_2$, and $Cu_2Se–SnSe_2$) of the title system have been well characterized.

Cu_2Se is a compound melting congruently at 1403 K and undergoing polymorphic transition at 396 K [28]. This compound has a homogeneity area extending toward an excess of selenium, which has the largest extent (33.3–36.6 at % Se) at 800 K.

Germanium diselenide $GeSe_2$ and tin diselenide $SnSe_2$ melt with an open maximum at 1015 [28] and 948 K [29] respectively.

Crystallographic data for the binary and ternary compounds of system A appear in Table 1.

System $Cu_2Se–GeSe_2$ forms ternary compounds Cu_8GeSe_6 and Cu_2GeSe_3 by a pertectic reaction (at 1083 K) and a dystectic reaction (at 1054 K), respectively [32]. Cu_8GeSe_6 experiences phase transition at 333 K [32] (or at 328 K [33]). Its low-temperature phase LT-Cu_8GeSe_6 crystallizes in hexagonal struc-

Table 1. Crystal data for compounds of the Cu_2Se–$GeSe_2$–$SnSe_2$ system

Compound, temperature range of existence, K	Structure	Space group	Unit cell parameters, nm	Source
HT-Cu_2Se, 396–1403	Cubic	$Fm3m$	$a = 0.5859(1)$	[28]
LT-Cu_2Se, <396	Monoclinic	$C2/c$	$a = 0.71379(4)$; $b = 1.23823(7)$; $c = 2.73904(9)$; $\beta = 94.308°$	[28]
$GeSe_2$, <1015	Monoclinic	$P2_1/c$	$a = 0.7016(5)$; $b = 1.6796(8)$; $c = 1.1831(5)$; $\beta = 90.65(5)°$	[27, 29]
$SnSe_2$, <948	Hexagonal	$P3m1$	$a = 0.3811$; $c = 0.6137$; $\gamma = 120°$	[27, 40]
HT-Cu_2GeSe_3, 1054–893	Orthorhombic	$Imm2$	$a = 1.1878(8)$; $b = 0.3941(3)$; $c = 0.5485(3)$	[33]
LT-Cu_2GeSe_3, <893	Tetragonal	$I42d$	$a = 0.55913(4)$; $c = 1.0977(1)$	[36]
HT-Cu_8GeSe_6, 1083–333	Cubic	$F\bar{4}3m$	$a = 1.1020$	[32]
LT-Cu_8GeSe_6, <333	Hexagonal	$P6_3mc$	$a = 1.26601(4)$; $c = 1.17698(3)$	[30, 31]
Cu_2SnSe_3, <968	Cubic	$F\bar{4}3m$	$a = 0.56877$	[41, 42]
	Monoclinic	$C2/c$	$a = 0.69670(3)$; $b = 1.20493(7)$; $c = 0.69453(3)$; $\beta = 109.19(1)°$	[43]

ture [32, 33], while the high-temperature phase HT-Cu_8GeSe_6 crystallizes in cubic structure [34] (Table 1). Cu_2GeSe_3 has two polymorphs with the phase transition at 893 K [35–38]. The high-temperature phase forms an orthorhombic lattice, and the low-temperature phase forms a tetragonal lattice. Two eutectics solidify in the system with the coordinates 1033 K, 38 mol % $GeSe_2$ and 973 K, 88 mol % $GeSe_2$ [32].

System Cu_2Se–$SnSe_2$ was studied in [39–41], and the results of those studies were summarized in the survey [42]. The system forms one compound, Cu_2SnSe_3, which melts congruently at 968 K [40, 41] and forms eutectics with the terminal binary components. The eutectic coordinates are 84 mol % $SnSe_2$, 853 K and 22 mol % $SnSe_2$, 983 K [40]. The solubility in the terminal compounds is within 3 mol % ($SnSe_2$) and 10 mol % (Cu_2Se) [41]. Cu_2SnSe_3 was reported to crystallize in a sphalerite-type cubic structure [43, 44]. However, the structural study of a single-crystal sample [45] showed that the compound has a monoclinic structure.

System $GeSe_2$–$SnSe_2$, which is a boundary quasi-binary system, has a eutectic phase diagram with limited reciprocal solubility in the terminal selenides [46]. The highest solubility in $GeSe_2$ and $SnSe_2$ is ~9.6 and 6 mol %, respectively, at the eutectic temperature (823 K). The eutectic melt contains 49 mol % $SnSe_2$.

EXPERIMENTAL

The terminal binary compounds (Cu_2Se, $SnSe_2$, and $GeSe_2$) and the terminal compounds (Cu_2GeSe_3, Cu_8GeSe_6, and Cu_2SnSe_3) of system A were prepared to be used in experiments.

The constituent elements used in experiments were high-purity samples purchased from Evochem Advanced Materials: granulated copper (Cu-00029, 99.9999%), germanium chips (Ge-00003, 99.9999%), granulated tin (Sn-00005, 99.999%), and granulated selenium (Se-00002, 99.999%). The binary and ternary compounds were prepared by alloying the constituent elements in stoichiometric proportions in evacuated (to ~10^{-2} Pa) and then sealed-off silica glass ampoules at temperatures slightly above the melting temperatures of the compounds to be prepared. Cu_2Se, $GeSe_2$, Cu_2GeSe_3, and Cu_8GeSe_6, whose melting temperatures far exceed the selenium boiling point (958 K [47]), were prepared in two-zone syntheses. An ampoule with the reaction mixture was heated in an inclined tube furnace to a temperature ~50 K higher than the melting point of the compound to be synthesized (a hot zone). A portion of the ampoule (~8 cm) was outside the furnace and cooled by water to control the selenium vapor pressure and avoid the ampoule explosion (a cold zone). The ampoule was rotated around its longitudinal axis and vibrated for speeding up the reaction. After most selenium was reacted, the ampoule was completely inserted into the furnace, exposed in the hot zone for 1 h, and then slowly cooled. In view of the deviation of Cu_2Se at low temperatures [28], the as-synthesized sample was quenched from 1300 K in cold water in order for it acquired a homogeneous stoichiometric composition.

DTA and X-ray powder diffraction were used to verify the identity of every compound prepared. The melting temperature and unit cell parameters for every

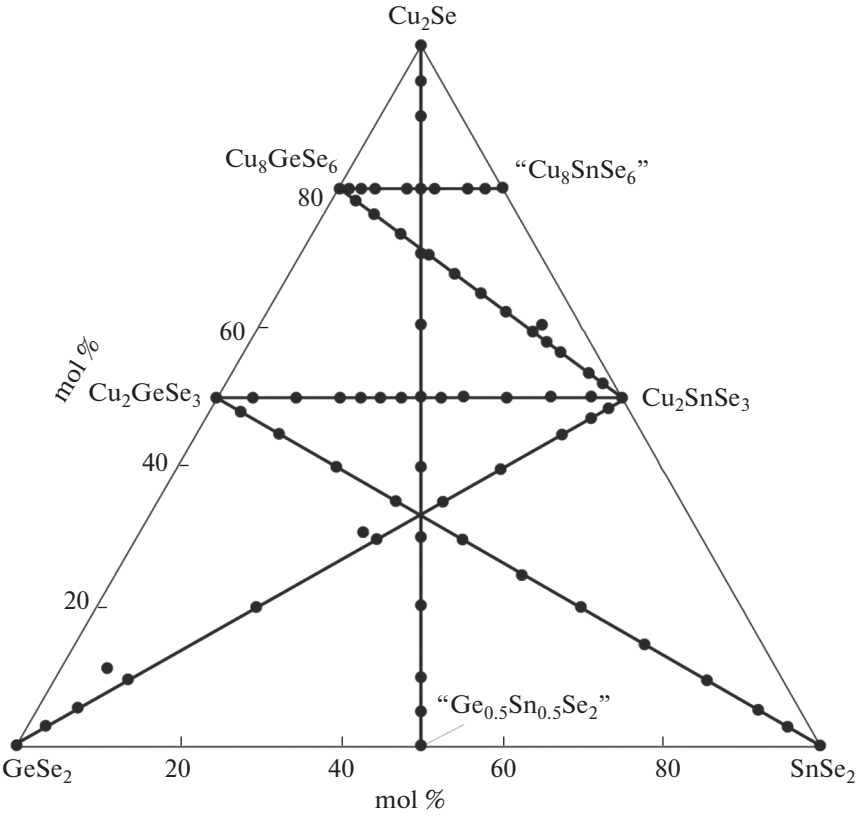

Fig. 1. Polythermal sections (lines) and alloys (dots) studied in the Cu_2Se–$GeSe_2$–$SnSe_2$ system.

prepared compound coincided with the above-cited literature data (Table 1) within the measurement error bars (DTA: ±3 K at high temperatures and ±2 at low temperatures; XRD: ±0.0003 Å).

More than 60 alloys to be used in experiments were prepared by direct in vacuo alloying of the terminal compounds; their compositions lie along Cu_2GeSe_3–Cu_2SnSe_3, Cu_8GeSe_6–"Cu_8SnSe_6," $0.4Cu_8GeSe_6$–Cu_2SnSe_3, $GeSe_2$–$0.5Cu_2SnSe_3$, $0.5Cu_2GeSe_3$–$SnSe_2$, and Cu_2Se–"$Ge_{0.5}Sn_{0.5}Se_2$" sections; some additional alloys were prepared beyond these sections (Fig. 1). In order to provide the conditions as close to equilibrium as possible, cast alloys that were prepared by rapid melt cooling were then annealed at 750 K for 500 h.

DTA experiments were carried out on a 404 F1 Pegasus System (Netzsch) differential scanning calorimeter. The heating rate was 10 K/min. In some cases, cooling curves were measured in order to determine the liquidus temperature. The DTA results were processed in the Netzsch Proteus Software. The temperature measurement accuracy was ±2°.

X-ray powder diffraction experiments were carried out at room temperature on a D8 Advance (Bruker) diffractometer using $CuK_{\alpha 1}$ radiation. X-ray diffraction patterns were indexed in the Topas V3.0 Software (Bruker).

RESULTS AND DISCUSSION

The joint processing of the experimental data set using the literature data on the Cu_2Se–$GeSe_2$ [32], Cu_2Se–$SnSe_2$ [39–42], and $GeSe_2$–$SnSe_2$ [46] boundary binary systems provided a self-consistent pattern of phase equilibria in the Cu_2Se–$GeSe_2$–$SnSe_2$ system.

Hereinafter in the text, tables, and figures, the following phase notations will be used:

- α and δ stand for HT-Cu_2Se-base and HT-Cu_8GeSe_6-base solid solutions, respectively;
- β_1 and β_2 stand for $GeSe_2$-base and $SnSe_2$-base solid solutions, respectively; and
- γ_1 and γ_2 stand for Cu_2GeSe_3-base and Cu_2SnSe_3-base solid solutions, respectively.

Quasi-Binary Section Cu_2GeSe_3–Cu_2SnSe_3

The DTA and XRD results on the Cu_2GeSe_3–Cu_2SnSe_3 system appear in Table 2. This system is a quasi-binary section of the quaternary system and has a peritectic-type phase diagram (Fig. 2). Peritectic equilibrium $L \leftrightarrow \gamma_1 + \gamma_2$ is acquired at 985 K. The peritectic point is at 60 mol % Cu_2SnSe_3.

Table 2. DTA data and unit cell parameters in the Cu_2GeSe_3–Cu_2SnSe_3 system

Composition, mol % Cu_2SnSe_3	DTA peak temperature, K	Crystal system, unit cell parameters, nm
0 (Cu_2GeSe_3)	1054	Tetragonal, $a = 0.39471$; $c = 0.54905$
10	1025–1045	
20	1005–1025	Tetragonal, $a = 0.39541$; $c = 0.55329$
30	990–1015	Tetragonal, $a = 0.39562$; $c = 0.55334$
35	987–1011	Tetragonal, $a = 0.39571$; $c = 0.55337$
40	985–1010	Tetragonal, $a = 0.39578$; $c = 0.5540$ (γ_1 phase) Cubic, $a = 0.5608$ (γ_2 phase)
		Tetragonal, $a = 0.39578$; $c = 0.5540$ (γ_1 phase) Cubic, $a = 0.5608$ (γ_2 phase)
45	985–1004	Cubic, $a = 0.56112$ Cubic, $a = 0.56223$
50	985–995	Cubic, $a = 0.56315$
55	981–990	
60	973–985	Cubic, $a = 0.56584$
70	970–980	
80	968–975	Cubic, $a = 0.56852$

The X-ray powder diffraction patterns of homogenized Cu_2GeSe_3–Cu_2SnSe_3 alloys verified the formation of extensive substitutional solid solutions. One can see in Fig. 3 that the powder diffraction pattern of a 20 mol % Cu_2SnSe_3 alloy is qualitatively identical to the diffraction pattern of the compound Cu_2GeSe_3. This implies that this alloy is a solid solution based on this compound (γ_1). The 60 and 80 mol % Cu_2SnSe_3 alloys have diffraction patterns identical to that of pure Cu_2SnSe_3 with reflection angles slightly shifting in response to changing composition. The diffraction patterns of these alloys are fully indexed in the cubic crystal system (space group $F\bar{4}3m$) with reflection angles slightly shifting in response to changing composition. The 40 mol % Cu_2SnSe_3 alloy is comprised of two phases; its diffraction pattern is the sum of the diffraction lines from the γ_1 and γ_2 phases. Noticeable is some broadening of the diffraction peaks from the solid solutions compared to those of the parent compounds. This is apparently owing to the crystal distortion caused by nonuniform Ge ↔ Sn substitution despite the long-term annealing. Table 2 lists the unit

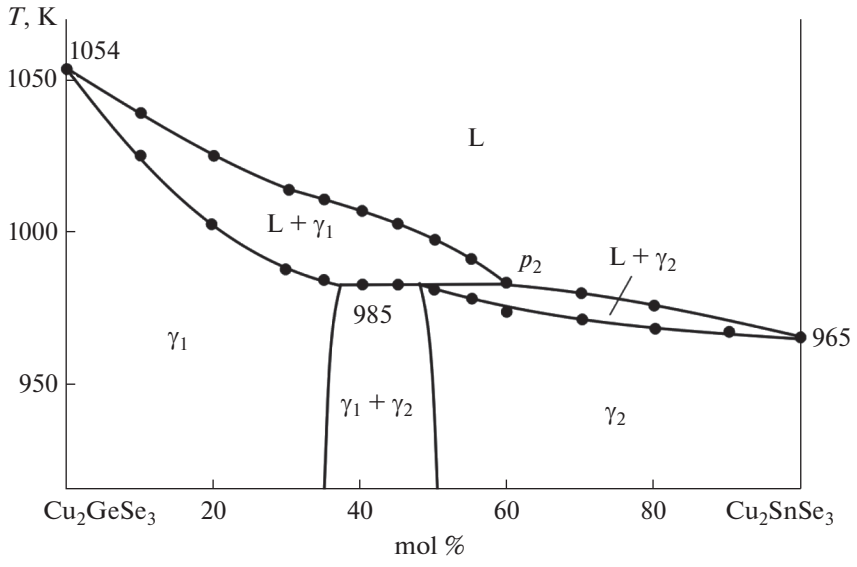

Fig. 2. Cu_2GeSe_3–Cu_2SnSe_3 phase diagram.

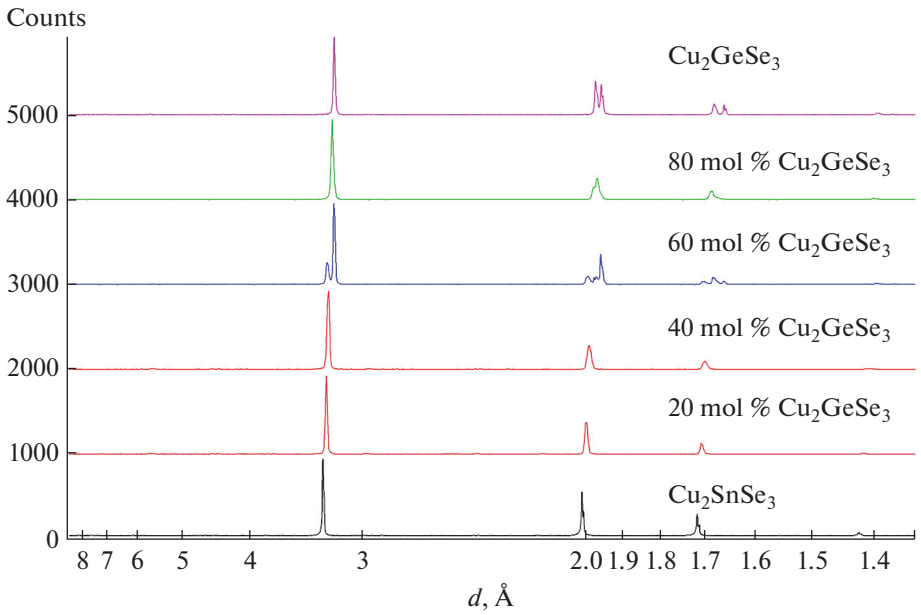

Fig. 3. X-ray powder diffraction patterns of Cu_2GeSe_3–Cu_2SnSe_3 alloys.

cell parameters of the alloys and parent compounds of the Cu_2GeSe_3–Cu_2SnSe_3 system calculated in the Topas V3.0 program; Fig. 4 displays their concentration dependecies. Figure 4 implies that the unit cell parameters of the γ_1 and γ_2 phases vary linearly in the range 0–35 and 50–100 mol % Cu_2SnSe_3, respectively, and in intemediate alloys they remain unchanged regardless of the general alloy composition. This impies that the end-members of mutually saturated γ_1 and γ_2 phases are 35 ± 1 and 50 ± 1 mol %, respectively.

Having indexed the powder diffraction patterns of Cu_2GeSe_3 and its base solid solutions and those of Cu_2SnSe_3 and its solid solutions, we found that the former were fully indexed in the tetragonal crystal system and the latter in the cubic crystal system.

Equilibrium Solid-Phase Diagram at 750 K

The equilibrium solid-phase diagram at 750 K was plotted using XRD data for some equilibrium alloys inside the Cu_2Se–$GeSe_2$–$SnSe_2$ concnetration triangle and the phase diagrams of boundary quasi-binary systems [32, 39–42, 46]. Figure 5 shows that the system features extensive solid solutions based on the terminal ternary compounds along the Cu_2GeS_3–Cu_2SnSe_3 quasi-binary section. The solid-solution homogeneity areas are shaped as bands with a width of ~1–2 mol % (for the γ_1 phase) and ~3–5 mol % (for the γ_2 phase). This correlates with the Cu_2Se–$GeSe_2$ and Cu_2Se–$SnSe_2$ phase diagrams [32, 42].

Limited solid solutions based on $GeSe_2$ (β_1), $SnSe_2$ (β_2), and HT-Cu_8GeSe_6 (δ) also exist in the system at 750 K. The β_1 and β_2 phases form narrow bands extending along the $GeSe_2$–$SnSe_2$ boundary quasi-binary system ~1 mol % wide and 8 and 6 mol % long, respectively. The δ phase homogeneity area extends to $Cu_8Ge_{0.9}Sn_{0.1}Se_6$ along the Cu_8GeSe_6–Cu_8SnSe_6 section. The solubility in the low-temeprature Cu_2Se phase is insignificant.

The interaction of coexisting phases in the system gives rise to two-phase areas ($\beta_1 + \gamma_1$, $\beta_2 + \gamma_2$, $\beta_2 + \gamma_1$, $\gamma_1 + \gamma_2$, $\gamma_1 + \delta$, $\gamma_2 + \delta$, $\gamma_2 + \alpha$, and $\alpha + \delta$) and three-phase areas ($\beta_1 + \beta_2 + \gamma_2$, $\beta_1 + \gamma_1 + \gamma_2$, $\gamma_1 + \gamma_2 + \delta$, $\alpha + \gamma_2 + \delta$). The phase compositions of samples in these fields were verified by XRD.

Figure 6 displays exemplary powder diffraction patterns of three alloys chosen from various phase areas (alloys 1, 2, and 3 in Fig. 5). An inspection of these diffraction patterns shows that they are the sums of diffraction lines from phases that are in equilibrium according to Fig. 5.

Liquids Surface Projection

Figure 7 images the liquidus surface projection of the Cu_2Se–$GeSe_2$–$SnSe_2$ system consisting of six primary crystallization fields of solid solutions based on binary compounds (α, β_1, and β_2) and ternary compounds (γ_1, γ_2, and δ). These fields are demarcated by eutectic and peritectic curves. On curve p_2U_1 at point K, peritectic equilibrium $L + \gamma_1 \leftrightarrow \gamma_2$ transforms to eutectic equilibrium $L \leftrightarrow \gamma_1 + \gamma_2$. These equilibria involve solid solutions. Therefore, in principle this transition must be accompanied by the formation of some surface in the relevant three-phase area, where

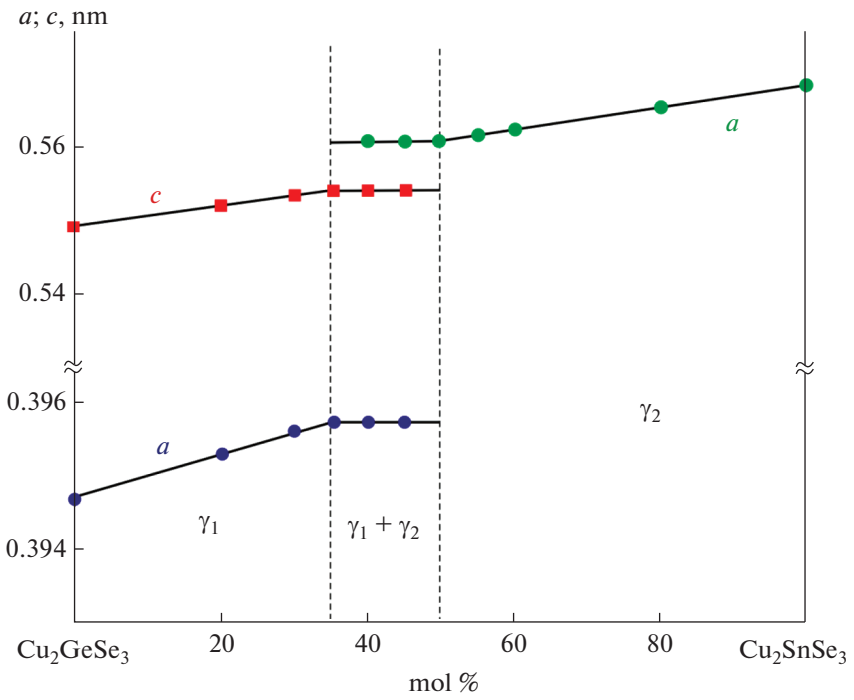

Fig. 4. Unit cell parameters versus concnetration in Cu_2GeSe_3–Cu_2SnSe_3 alloys.

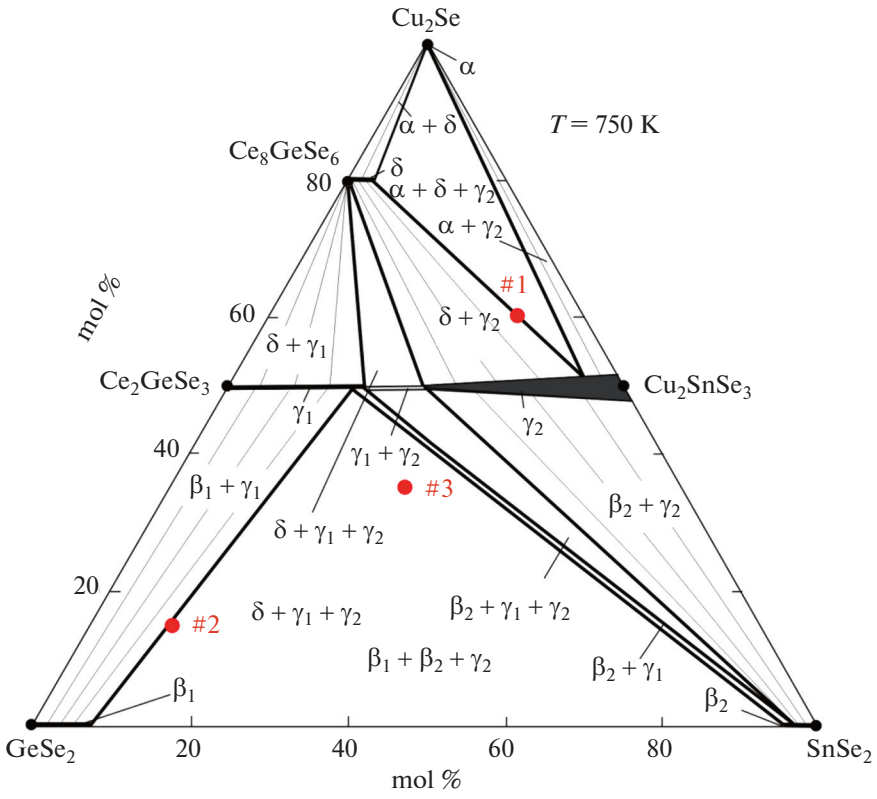

Fig. 5. 750-K isotherm of the Cu_2Se–$GeSe_2$–$SnSe_2$ system.

Table 3. Invariant equilibria in the $Cu_2Se–GeSe_2–SnSe_2$ system

Point in Fig. 6	Equilibrium	Composition, mol %		T, K
		Cu_2Se	$SnSe_2$	
D_1	$L \leftrightarrow Cu_2GeSe_3$	50	–	1054
D_2	$L \leftrightarrow Cu_2SnSe_3$	50	50	965
p_1	$L + \alpha \leftrightarrow \delta$	75	–	1080
p_2	$L + \gamma_1 \leftrightarrow \gamma_2$	50	30	985
e_1	$L \leftrightarrow \gamma_1 + \beta_1$	15	–	975
e_2	$L \leftrightarrow \gamma_1 + \delta$	60	–	1030
e_3	$L \leftrightarrow \alpha + \gamma_2$	75	25	940
e_4	$L \leftrightarrow \gamma_2 + \beta_2$	18	82	860
e_5	$L \leftrightarrow \beta_1 + \beta_2$	5	49	815
U_1	$L + \gamma_2 \leftrightarrow \beta_2 + \gamma_1$	12	55	845
U_2	$L + \gamma_1 \leftrightarrow \delta + \gamma_2$	57	27	965
U_3	$L + \delta \leftrightarrow \alpha + \gamma_{21}$	73	24	950
E	$L \leftrightarrow \beta_1 + \beta_2 + \gamma_1$	5	48	805

three-phase equilibrium would become two-phase equilibrium with a passive role of the third phase [48, 49]. Since the γ_1 and γ_2 homogeneity areas almost do not go beyond the $Cu_2GeSe_3–Cu_2SnSe_3$ quasi-binary section, this surface is most likely degenerates into a point (K).

The types and coordinates of invariant equilibria and the types and temperature ranges of monovariant equilibria appear in Tables 3 and 4, respectively.

The $Cu_2GeSe_3–Cu_2SnSe_3$ quasi-binary section divides the $Cu_2Se–GeSe_2–SnSe_2$ concnetration triangle into a pair of independent subsystems: $Cu_2Se–Cu_2GeSe_3–Cu_2SnSe_3$ and $GeSe_2–Cu_2GeSe_3–Cu_2SnSe_3$. The former features two invariant transition reactions (U_2 and U_3), and the latter features one invariant transition equilibrium (U_1) and one eutectic equilibrium (E). Noteworthy, the latter can be regarded the reciprocal system $1.5GeSe_2 + Cu_2SnSe_3 \leftrightarrow 1.5SnSe_2 + Cu_2GeSe_3$. Figure 7 implies that it is a reversibly reciprocal system, that is, it has not a quasi-binary diagonal. This is owing to the fact that the terminal compounds do not play a decisive role in the distrobution of phase areas, but their base extensive solid-solutions areas do.

Polythermal Sections of the Phase Diagram

Below we will consider some polythermal sections of the phase diagram of the title system in the context of the liquidus surface projection (Fig. 7; Tables 3 and 4) and the 750-K solid-phase equilibrium diagram (Fig. 5).

Section Cu_8GeSe_6–"Cu_8SnSe_6" (Fig. 8) entirely lies in the α phase primary crystallization area. The primary crystallization of the α phase is followed by crystallization of the HT-Cu_8GeSe_6-base δ phase by peritectic reaction $L + \alpha \leftrightarrow \delta$ and the crystallziation of $\alpha + \gamma_2$ two-phase mixtures by eutectic reaction $L \leftrightarrow \alpha + \gamma_2$ (Table 4; Fig. 7, curves p_1U_3 and U_3e_3).

The specificity of this section is in the δ phase homogeneity area lying on its plane, so that peritectic reaction $L + \alpha \leftrightarrow \delta$ fully consumes both initial phases simultaneously. It is for this reason that this peritectic

Table 4. Monovariant equilibria in the $Cu_2Se–GeSe_2–SnSe_2$ system

Curve in Fig. 6	Equilibrium	Temperature range, K
e_1E	$L \leftrightarrow \beta_1 + \gamma_1$	975–805
e_5E	$L \leftrightarrow \beta_1 + \beta_2$	815–805
e_4U_1	$L \leftrightarrow \beta_2 + \gamma_2$	860–845
U_1E	$L \leftrightarrow \beta_2 + \gamma_1$	845–805
e_2U_2	$L \leftrightarrow \gamma_1 + \delta$	1030–965
p_2K	$L + \gamma_1 \leftrightarrow \gamma_2$	985–925
KU_1	$L \leftrightarrow \gamma_1 + \gamma_2$	925–845
p_2U_2	$L + \gamma_1 \leftrightarrow \gamma_2$	985–965
U_2U_3	$L + \delta \leftrightarrow \gamma_2$	965–950
p_1U_3	$L + \alpha \leftrightarrow \delta$	1080–950
U_3e_3	$L \leftrightarrow \alpha + \gamma_2$	950–940

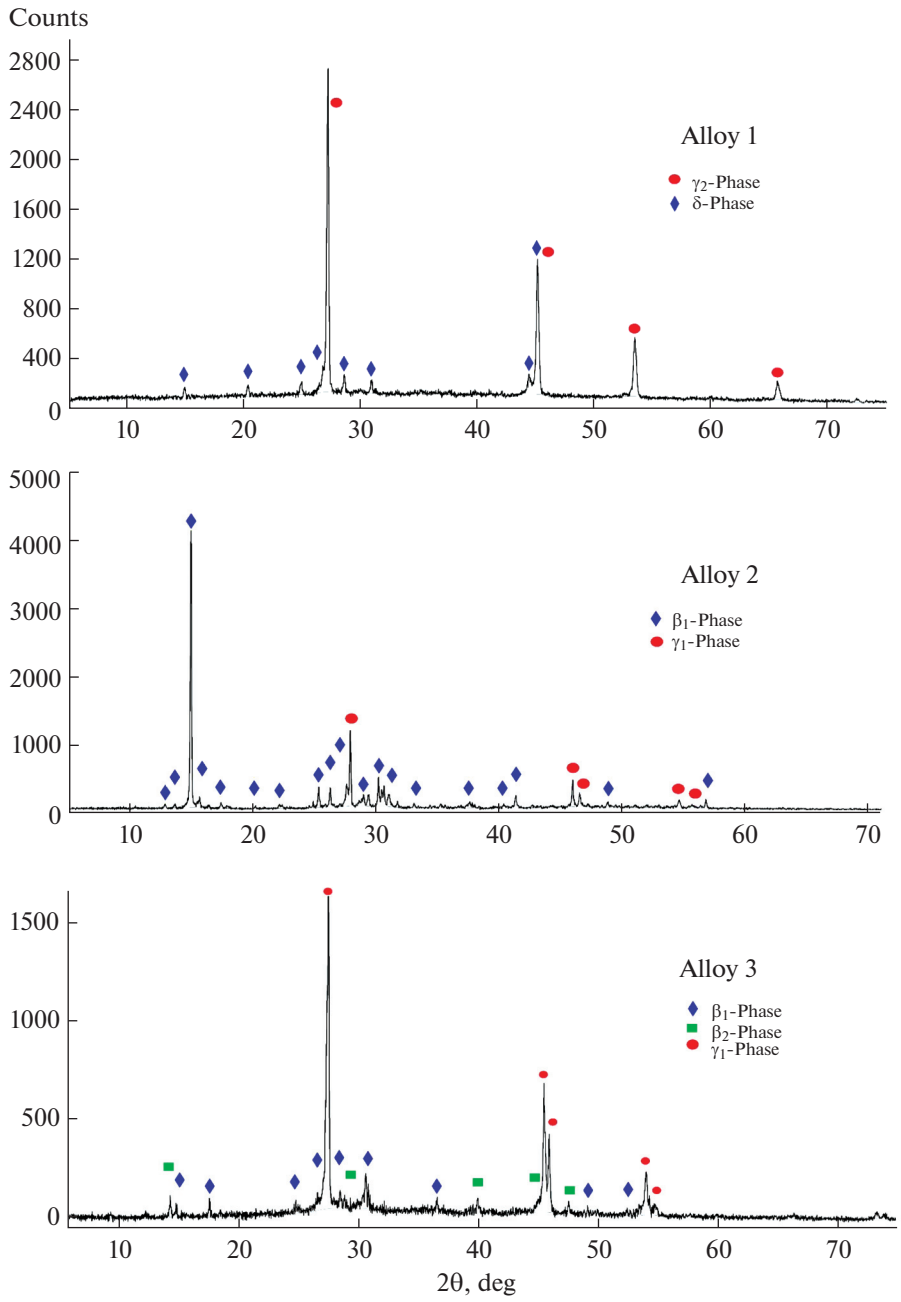

Fig. 6. X-ray powder diffraction patterns and phase compositions of selected Cu_2Se–$GeSe_2$–$SnSe_2$ alloys. Alloy 1: 60 mol % Cu_2Se + 9 mol % $GeSe_2$; alloy 2: 15 mol % Cu_2Se + 75 mol % $GeSe_2$; and alloy 3: 35 mol % Cu_2Se + 35 mol % $GeSe_2$.

reaction in Cu_8GeSe_6-rich compositions ends by the formation of δ solid solutions, which immediately border the L + α + δ three-phase area (Fig. 8). In 15–85 mol % compositions, crystallization ends by invariant transition reaction L + δ ↔ α + γ_2 (U_3) to form the α + δ + γ_2 three-phase subsolidus area.

Section 0.4Cu_8GeSe_6–Cu_2SnSe_3 (Fig. 9) crosses the primary crystallization fields of the α phase (0–15 mol % Cu_2SnSe_3), δ phase (15–50 mol % Cu_2SnSe_3), and γ_2 phase (50–100 mol % Cu_2SnSe_3). The α phase primary crystallization is followed by peritectic monovariant reaction L + α ↔ δ, which gives rise to the L + α + δ three-phase area. This reaction ends at ~1040 K by an excess of the liquid phase and the formation of the L + δ two-phase area. In this area, crystallization ends by reaction L + δ ↔ γ_2 (Table 4, U_2U_3), and the δ + γ_2 two-phase area appears in the subsolidus.

In the 45–80 mol % Cu_2SnSe_3 range, transition reaction L + δ ↔ α + γ_2 (Table 3, U_3) ends with an

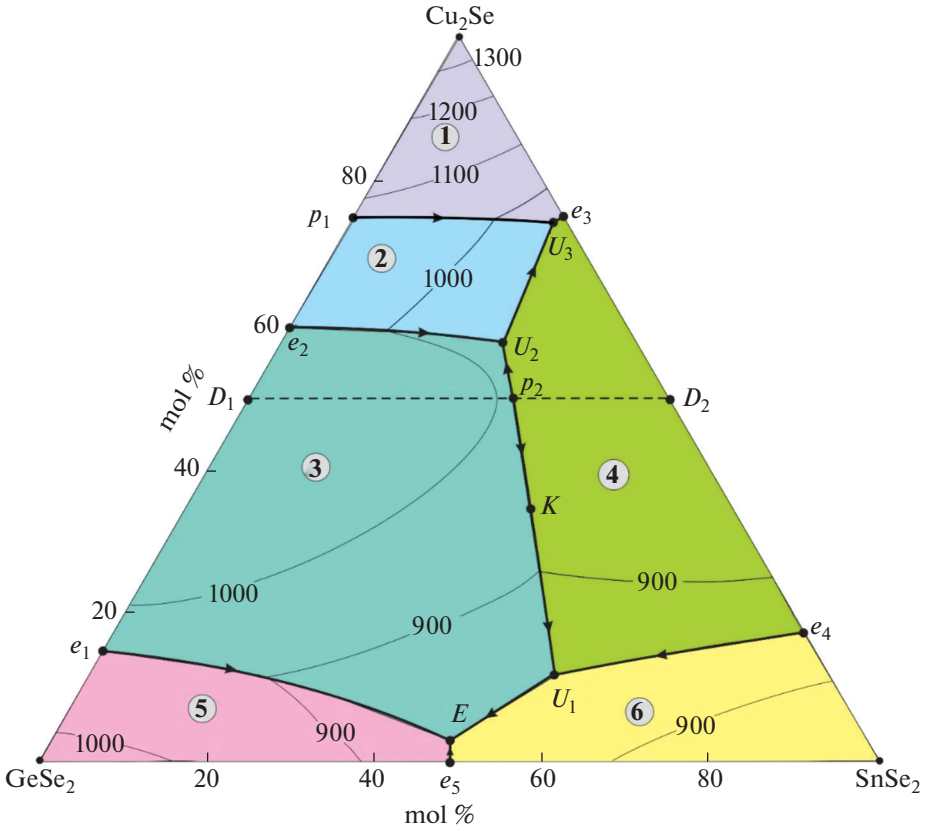

Fig. 7. Liquidus surface projection for the $Cu_2Se–GeSe_2–SnSe_2$ system. Primary crystallization fields: (1) α (Cu_2Se), (2) δ (Cu_8GeSe_6), (3) γ_1 (Cu_2GeSe_3), (4) γ_2 (Cu_2SnSe_3), (5) β_1 ($GeSe_2$), and (60) β_2 ($SnSe_2$).

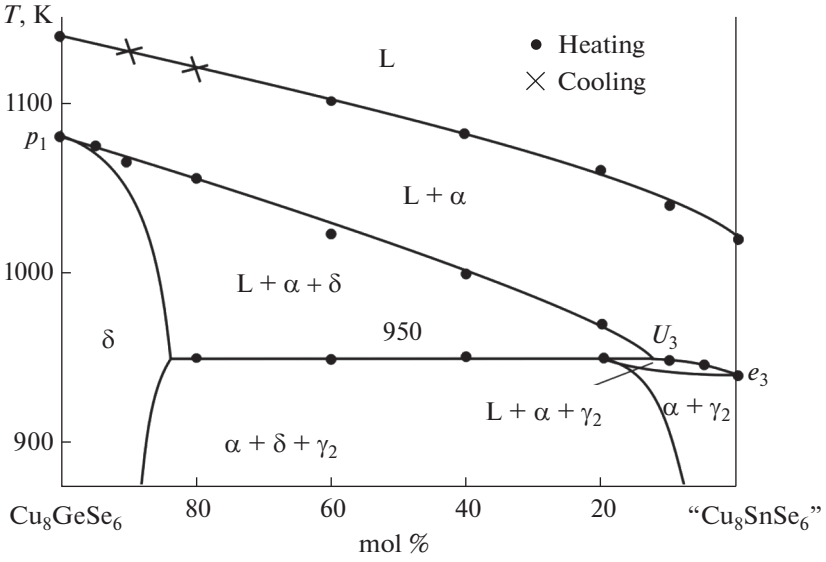

Fig. 8. Polythermal section Cu_8GeSe_6–"Cu_8SnSe_6."

excess of the δ phase to form the α + δ + γ_2 three-phase area. In Cu_2SnSe_3-rich areas, crystallization ends by L ↔ γ_2 and L ↔ α + $?_2$ equilibria (Table 4, U_3e_3).

Section $GeSe_2$–0.5Cu_2SnSe_3 (Fig. 10) has a liquidus of three branches that correspond to the primary crystallization of the β_1, γ_1, and γ_2 phases. Their intersection points correspond to the onset of a monovari-

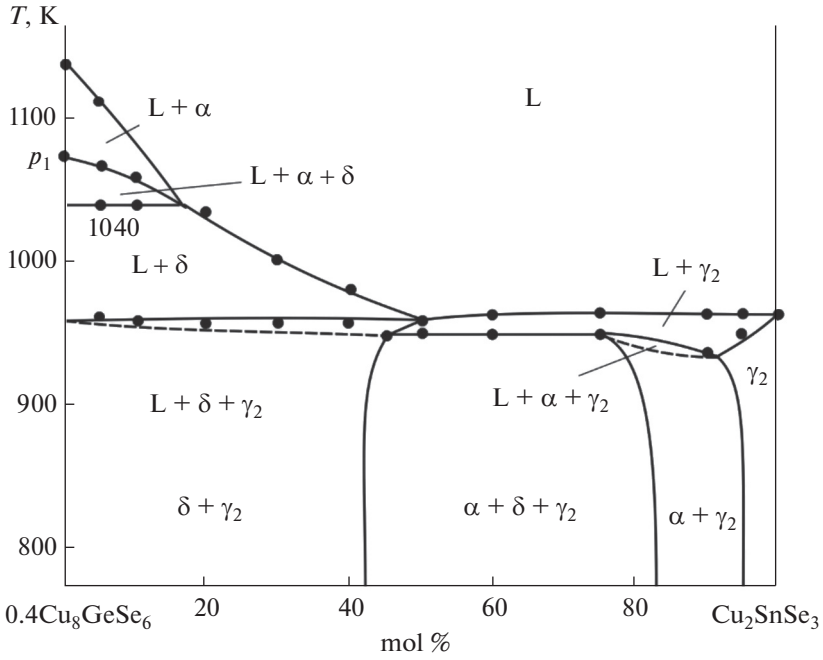

Fig. 9. Polythermal section $0.4Cu_8GeSe_6$–Cu_2SnSe_3.

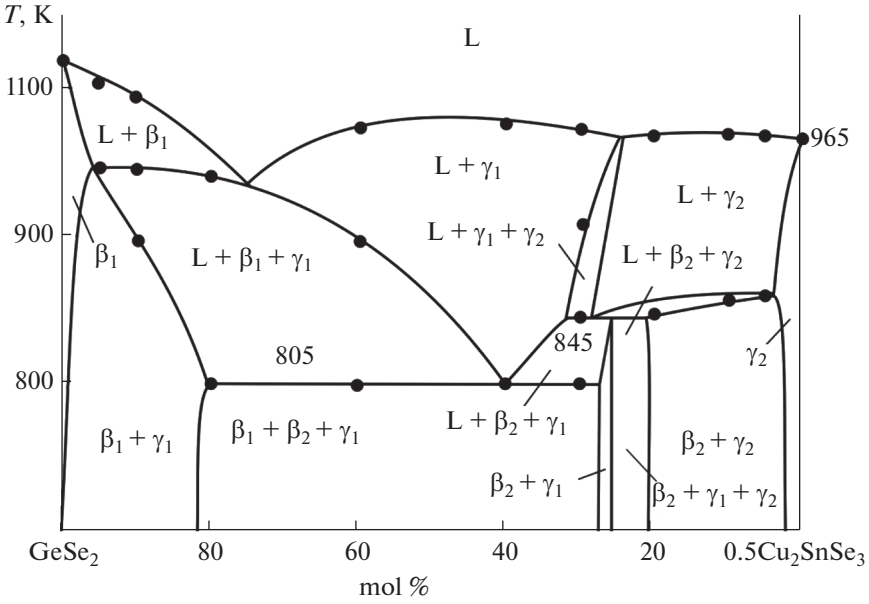

Fig. 10. Polythermal section $GeSe_2$–$0.5Cu_2SnSe_3$.

ant peritectic reaction (p_2K) and a eutectic reaction (e_1E). The L + β_1 + γ_1 and L + γ_1 + γ_2 three-phase areas are formed as a result of these reactions. In the 80–95 mol % $GeSe_2$ area, crystallization ends by peritectic reaction p_2K and to form the β_1 + γ_1 two-phase area.

The γ_2 phase primary crystallization field continues by the eutectic monovariant scheme L $\leftrightarrow$ β_2 + γ_2 (e_4U_1) and ends in the 5–20 mol % $GeSe_2$ range to form the β_2 + γ_2 two-phase area. In the 20–25 mol % $GeSe_2$ narrow concentration range, crystallization ends by transition reaction U_1 (845 K) to form the β_2 + γ_1 + γ_2 three-phase area.

The 805-K horizontal (E) corresponds to the invariant solidification of the β_1 + β_2 + γ_1 ternary eutectic.

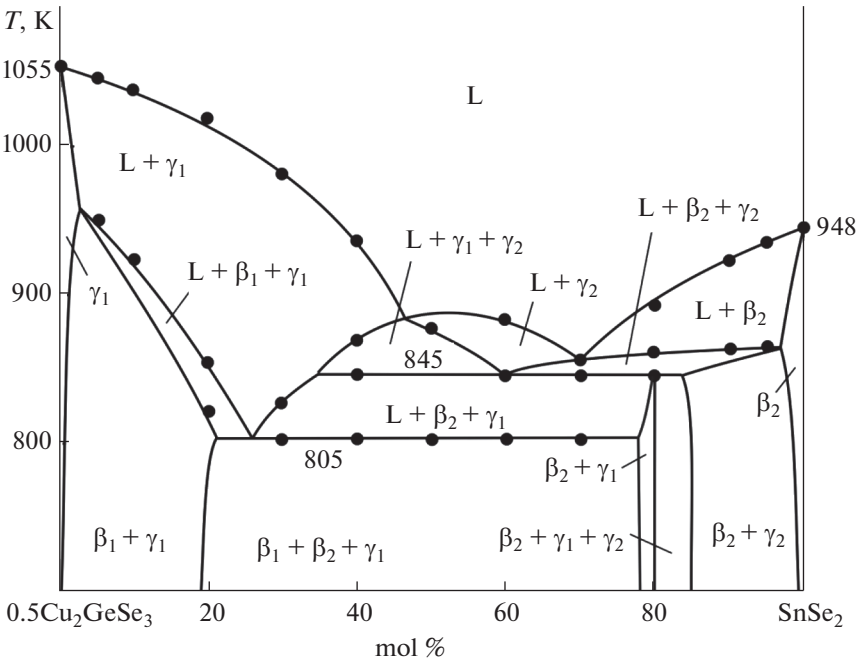

Fig. 11. Polythermal section $0.5Cu_2SnSe_3$–$SnSe_2$.

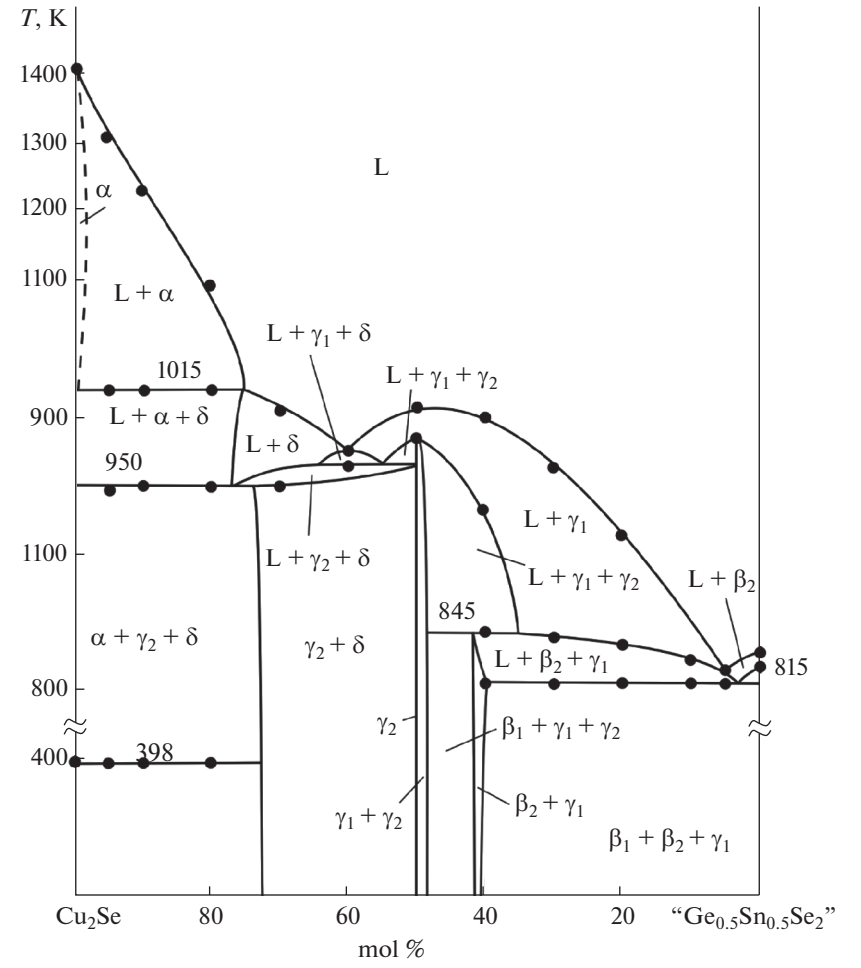

Fig. 12. Polythermal section Cu_2Se–$Ge_{0.5}Sn_{0.5}Se_2$.

Section $0.5Cu_2GeSe_3$–$SnSe_2$ (Fig. 11) crosses the primary crystallization fields of the γ_1, γ_2, and β_2 phases. Below liquidus, there are monovariant equilibria (e_1E, U_1E, KU_1, and e_4U_1) and invariant equilibria (U_1 and E). When the crystallization is over, a series of two- and three-phase mixtures are formed by these reactions.

Section Cu_2Se–$Ge_{0.5}Sn_{0.5}Se_2$ (Fig. 12) passes through the primary crystallization fields of the α, δ, γ_1, and γ_2 phases; in the subsolidus, it crosses four three-phase areas. Phase equilibria along this section can easily be recognized by comparing Fig. 11 with Figs. 4 and 6. The T–x diagram of this section clearly features transition invariant equilibria U_1, U_2, U_3, and E (horizontals at 845, 965, 950, and 805 K, respectively). The 398-K horizontal corresponds to the $\alpha \leftrightarrow$ LT-Cu_2Se polymorphic transition.

CONCLUSIONS

We have elucidated the full pattern of phase equilibria in the Cu_2Se–$GeSe_2$–$SnSe_2$ quasi-ternary system, involving the solid-phase diagram at 750 K, the liquidus surface projection, and a series of polythermal sections of the phase diagram. Extensive solid solutions have been found to exist in the system along the Cu_2GeSe_3–Cu_2SnSe_3 quasi-binary section. Primary crystallization and homogeneity areas of phases have been determined, as well as the characters and types of invariant and monovariant equilibria in the title system. The prepared new phases of variable composition are of interest as environmentally safe candidate thermoelectric materials.

FUNDING

The work was supported by the Science Development Foundation under the President of the Azerbaijan Republic (project No. EİF-BGM-4-RFTF-1/2017-21/11/4-M-12).

CONFLICT OF INTEREST

The authors declare that they have no conflicts of interest.

REFERENCES

1. X. L. Sanghoon, L. J. Tengfei, and L. Zhang, Y-H. *Chalcogenide: From 3D to 2D and Beyond* (Elsevier, 2019). https://doi.org/10.1016/C2017-0-03585-1.
2. X. Chen, J. Yang, T. Wu, et al., Nanoscale **10**, 15130 (2018). https://doi.org/10.1039/C8NR05558
3. E. Peccerillo and K. Durose, MRS Energy Sustainability **5**, 1 (2018). https://doi.org/10.1557/mre.2018.10
4. B. Yun, H. Zhu, J. Yuan, et al., J. Mater. Chem. B **8**, 4778 (2020). https://doi.org/10.1039/D0TB00182A
5. Z. Xia, H. Fang, X. Zhang, et al., Chem. Mater. **30**, 1121 (2018). https://doi.org/10.1021/acs.chemmater.7b05104
6. T. R. Wei, Y. Qin, T. Deng, et al., Sci. China Mater. **62**, 8 (2019). https://doi.org/10.1007/s40843-018-9314-5
7. A. Mikula, K. Mars, P. Nieroda, and P. Rutkowski, Materials **14**, 2635 (2021). https://doi.org/10.3390/ma14102635
8. T. Deng, P. Qiu, and T. Xing, J. Mater. Chem. A **9**, 7946 (2021). https://doi.org/10.1039/D0TA12042A
9. B. Jiang, P. Qiu, E. Eikeland, et al., J. Mater. Chem. C **5**, 943 (2017). https://doi.org/10.1039/c6tc05068a
10. M. Siyar, J. -Y. Cho, Y. Youn, et al., J. Mater. Chem. C **6**, 1780 (2018). https://doi.org/10.1039/C7TC05180H
11. R. Chetty, D. S. Prem-Kumar, M. Falmbigl, et al., Intermetallics **54**, 1 (2014). https://doi.org/10.1016/j.intermet.2014.05.006
12. A. K. Ivanov-Shchits and I. V. Murin, *Solid State Ionics*, vol. 1 (Izd-vo St. Peterb. Univ., St. Petersburg, 2000) [in Russian].
13. V. M. Berezin and G. P. Vyatkin, *Superionic Semiconductor Chalcogenides* (Chelyabinsk, 2001) [in Russian].
14. H. Liu, X. Shi, F. Xu, et al., Nature Materials **11**, 422 (2012). https://doi.org/10.1038/nmat3273
15. M. B. Babanly, Yu. A. Yusibov, and V. T. Abishev, *Three-Component Chalcogenides Based on Copper and Silver* (Baku, 1993) [in Russian].
16. M. B. Babanly, Yu. A. Yusibov, and N. B. Babanly, in *Electromotive Force and Measurement in Several Systems*, Ed. by S. Kara (IntechOpen, 2011). https://doi.org/10.5772/28934
17. X. Liang, Appl. Phys. Lett. **111**, 133902 (2017). https://doi.org/10.1063/1.4997501
18. P. Qiu, M. T. Agne, Y. Liu, et al., Nature Commun. **9** (2910) (2018). https://doi.org/10.1038/s41467-018-05248-8
19. M. B. Babanly, L. F. Mashadiyeva, D. M. Babanly, et al., Russ. J. Inorg. Chem. **64**, 1134 (2019). https://doi.org/10.1134/S0036023619130035
20. M. B. Babanly, E. V. Chulkov, Z. S. Aliev, et al., Russ. J. Inorg. Chem. **62**, 1703 (2017). https://doi.org/10.1134/S0036023617130034
21. V. P. Zlomanov, A. M. Khoviv, and A. Yu. Zavrazhnov, in *Materials Science – Advanced Topics* (IntechOpen, 2013). https://doi.org/10.5772/56700
22. S. Z. Imamaliyeva, D. M. Babanly, D. B. Tagiev, and M. B. Babanly, Russ. J. Inorg. Chem. **13**, 1703 (2018). https://doi.org/10.1134/S0036023618130041
23. I. J. Alverdiyev, Z. S. Aliev, S. M. Bagheri, et al., J. Alloys Compd. **691**, 255 (2017). https://doi.org/10.1016/j.j

24. L. F. Mashadiyeva, Z. T. Gasanova, Yu. A. Yusibov, and M. B. Babanly, Russ. J. Inorg. Chem. **62**, 598 (2017). https://doi.org/10.1134/S0036023617050151
25. Z. T. Gasanova, L. F. Mashadiyeva, Yu. A. Yusibov, and M. B. Babanly, Russ. J. Inorg. Chem. **62**, 591 (2017). https://doi.org/10.1134/S0036023617050126
26. L. F. Mashadieva, Z. T. Gasanova, Yu. A. Yusibov, and M. B. Babanly, Inorg. Mater. **54**, 8 (2018). https://doi.org/10.1134/S0020168518010090
27. E. N. Ismailova, L. F. Mashadieva, I. B. Bakhtiyarly, and M. B. Babanly, Russ. J. Inorg. Chem. **64**, 801 (2019). https://doi.org/10.1134/S0036023619060093
28. *Binary Alloy Phase Diagrams*, Ed. by T. B. Massalski T. B. (ASM International, Materials Park, Ohio, 1990). https://doi.org/10.1002/adma.19910031215
29. N. Kh. Abrikosov, in *Semiconductor Physics* (Springer, 2013). https://doi.org/10.1007/978-1-4899-6373-4.
30. L. Gulay, M. Daszkiewicz, O. Strok, and A. Pietraszko, Chem. Met. Alloys **4**, 200 (2011). https://doi.org/10.30970/cma4.0184
31. G. Dittmar and H. Schafer, Acta Crystallogr. **32**, 2726 (1976). https://doi.org/10.1107/s0567740876008704
32. V. Tomashik, Copper-Germanium-Selenium, Ternary Alloys VCH **2**, 288 (2015).
33. M. Onoda, M. Ishii, P. Pattison, et al., J. Solid State Chem. **146**, 355 (1999). https://doi.org/10.1006/jssc.1999.8362
34. V. N. Moroz, Izv. Akad. Nauk SSSR, Neorg. Mater. **26**, 1830 (1990).
35. G. Marcano and L. Ieves, J. Appl. Phys. **87**, 1284 (2000). https://doi.org/10.1063/1.372010
36. O. V. Parasyuk, L. D. Gulay, Ya. E. Romanyuk, and L. V. Piskach, J. Alloys Compd. **329**, 202 (2001). https://doi.org/10.1016/s0925-8388(01)01606-1
37. O. S. Lychmanyuk, L. D. Gulay, I. D. Olekseyuk, et al., Pol. J. Chem. **81**, 353 (2007).
38. B. B. Sharma, Phys. Status Solidi A **2**, 13 (1970). https://doi.org/10.1002/pssa.19700020125
39. J. Rivet, P. Laruelle, and J. Flahaut, Bull. Soc. Chim. Fr. **5**, 1667 (1970).
40. L. I. Berger and E. K. Kotina, Inorg. Mater. (Engl. Trans.) **9**, 330 (1973).
41. T. V. Zotova and Yu. A. Karagodin, Sb. Nauchn. Trudov Probl. Mikroel. **21**, 57 (1975).
42. I. D. Olekseyuk, O. V. Parasyuk, L. V. Piskach, et al., *Quasi-Ternary Systems of Chalcogenides* (Vega Publish, Lutsk, 1999).
43. L. S. Palatnik, Yu. F. Komnik, E. K. Belova, and L. V. Atroshchenko, Kristallografiya **6**, 960 (1961).
44. B. B. Sharma, R. Ayyar, and H. Singh, Phys. Status Solidi A **40**, 691 (1977). https://doi.org/10.1002/pssa.2210400237
45. G. Marcano, L. M. de Chalbaud, C. Rincon, and G. Sanchez-Perez, Mater. Lett. **53**, 151 (2002). https://doi.org/10.1016/S0167-577X(01)00466-9
46. M. I. Karakhanova, L. P. Sokolova, and A. V. Novoselova, Izv. Akad. Nauk SSSR, Neorgan. Mater. **12**, 1221 (1976).
47. J. Emsley, *The Elements* (Clarendon Press, Oxford, 1991).
48. V. I. Lutsyk, V. P. Vorob'eva, and S. Ya. Shodorova, Russ. J. Phys. Chem. **89**, 2331 (2015). https://doi.org/10.1134/S0036024415130245
49. V. I. Lutsyk and V. P. Vorob'eva, Russ. J. Phys. Chem. A **91**, 2593 (2017). https://doi.org/10.1134/S0036024417130131

Translated by O. Fedorova